

Impact of assimilating Taiwan's coastal radar radial velocity on forecasting Typhoon Morakot (2009) in southeastern China using a WRF-based EnKF

YUE Jian & MENG ZhiYong*

Laboratory for Climate and Ocean-Atmosphere Studies, Department of Atmospheric and Oceanic Sciences, School of Physics, Peking University, Beijing 100871, China

Received May 17, 2016; accepted July 1, 2016; published online November 17, 2016

Abstract This study explores for the first time the impact of assimilating radial velocity (Vr) observations from a single or multiple Taiwan's coastal radars on tropical cyclone (TC) forecasting after landfall in the Chinese mainland by using a Weather Research and Forecasting model (WRF)-based ensemble Kalman filter (EnKF) data assimilation system. Typhoon Morakot (2009), which caused widespread damage in the southeastern coastal regions of the mainland after devastating Taiwan, was chosen as a case study. The results showed that assimilating Taiwan's radar Vr data improved environmental field and steering flow and produced a more realistic TC position and structure in the final EnKF cycling analysis. Thus, the subsequent TC track and rainfall forecasts in southeastern China were improved. In addition, better observations of the TC inner core by Taiwan's radar was a primary factor in improving TC rainfall forecast in the Chinese mainland.

Keywords Radial velocity, EnKF, TC track forecast, Rainfall forecast, Chinese mainland

Citation: Yue J, Meng Z Y. 2017. Impact of assimilating Taiwan's coastal radar radial velocity on forecasting Typhoon Morakot (2009) in southeastern China using a WRF-based EnKF. *Science China Earth Sciences*, 60: 315–327, doi: 10.1007/s11430-015-0259-y

1. Introduction

On average, seven tropical cyclones (TCs) make landfall in the mainland of China per year, causing an average of 472 fatalities and 28.7 billion RMB in direct economic losses (Zhang Q et al., 2009), mainly due to the heavy rainfall associated with TCs and fresh flooding. However, forecasting TCs that make landfall is a major challenge in both research and operational communities, probably because of the inaccuracy of initial TC conditions such as structure and location. In particular, heavy rainfall associated with TCs is often poorly predicted by numerical models (Houze et al., 2007; Gao et al., 2009).

One major reason for the low rainfall forecast skill of the

numerical models is the error in the initial vortex structure arising from the lack of TC inner-core observations over the open ocean. When a TC is approaching landfall, coastal radar can cover an area of up to 460 km offshore, and thus may be an important data source for improving the TC initial structure analysis and subsequent heavy rainfall forecast at and after landfall. Previous studies have shown that assimilating coastal radar data improved the rainfall forecast of hurricanes making landfall in the Atlantic basin by using either three-dimensional variational data assimilation (3DVar; e.g., Zhao and Jin, 2008; Zhao and Xue, 2009; Li et al., 2012) or the ensemble Kalman filter (EnKF) techniques (e.g., Dong and Xue, 2013).

In the western North Pacific, about 73% of TCs that made landfall in the Chinese mainland in the past 10 years passed within 500 km of Taiwan. Ground-based radars in Taiwan may provide information about the inner structure of TCs

*Corresponding author (email: zymeng@pku.edu.cn)

much earlier than coastal radars in the Chinese mainland. Zhao et al. (2012) obtained a skillful rainfall forecast in southeastern China for Typhoon Meranti (2010) through assimilating radial velocity (V_r) and reflectivity data from coastal radars in both Taiwan and coastal regions of the Chinese mainland with a 3DVar system. As yet, the impact of EnKF-based data assimilation (DA) of Taiwan's radar on the TC track and rainfall forecasts after a TC makes landfall in the mainland of China has not been examined.

Over the past decade, numerous studies have demonstrated that numerical model forecasts initiated with an EnKF are superior to those initiated with a 3DVar method (e.g., Meng and Zhang, 2008a, 2008b; Whitaker et al., 2008; Zhang F Q et al., 2009, hereafter Z09; Hamill et al., 2011; Zhang et al., 2011). 3DVar uses static isotropic background error covariance, whereas the EnKF estimates flow-dependent background error covariance through an ensemble of short-term forecasts (Hamill and Whitaker, 2005).

In this work, we examine the impact of assimilating V_r of Taiwan's coastal radars on the forecast of Typhoon Morakot (2009) in southeastern China using a Weather Research and Forecasting model (WRF)-based EnKF. Although Morakot was most notable for the extremely heavy rainfall and subsequent mudslides that it caused in Taiwan (Wu, 2013; Yu and Cheng, 2013), it also caused heavy rainfall in southeastern China upon its second landfall, which resulted in nine fa-

talities, 8.9 billion RMB direct economic losses, and the destruction of nearly 6000 homes (Wu and Yang, 2011). However, the official 24-h rainfall forecast after Morakot's second landfall issued by the China National Meteorological Center (CNMC) had a severe location bias, and missed the heavy rainfall (Figure 1a and 1b).

2. Review of Typhoon Morakot and Doppler radar data

2.1 Review of Typhoon Morakot (2009)

Typhoon Morakot formed as a tropical depression east of Taiwan early on 2 August 2009 and became a tropical storm at 1800 UTC 3 August. The storm gradually intensified as it tracked westward, and reached typhoon strength at 1200 UTC 5 August. Morakot weakened slightly as it made first landfall near Hua-Lien on the east coast of Taiwan at around 1800 UTC 7 August. After crossing northern Taiwan, Morakot moved slowly north-northwest over the Taiwan Strait at around 0600 UTC 8 August, remaining as a severe tropical storm until its second landfall in Fujian Province at around 1200 UTC 9 August. Thereafter, Morakot gradually weakened as it moved slowly northward inland and eventually dissipated on 11 August. After Morakot's second landfall, heavy rainfall was observed in Fujian, Zhejiang,

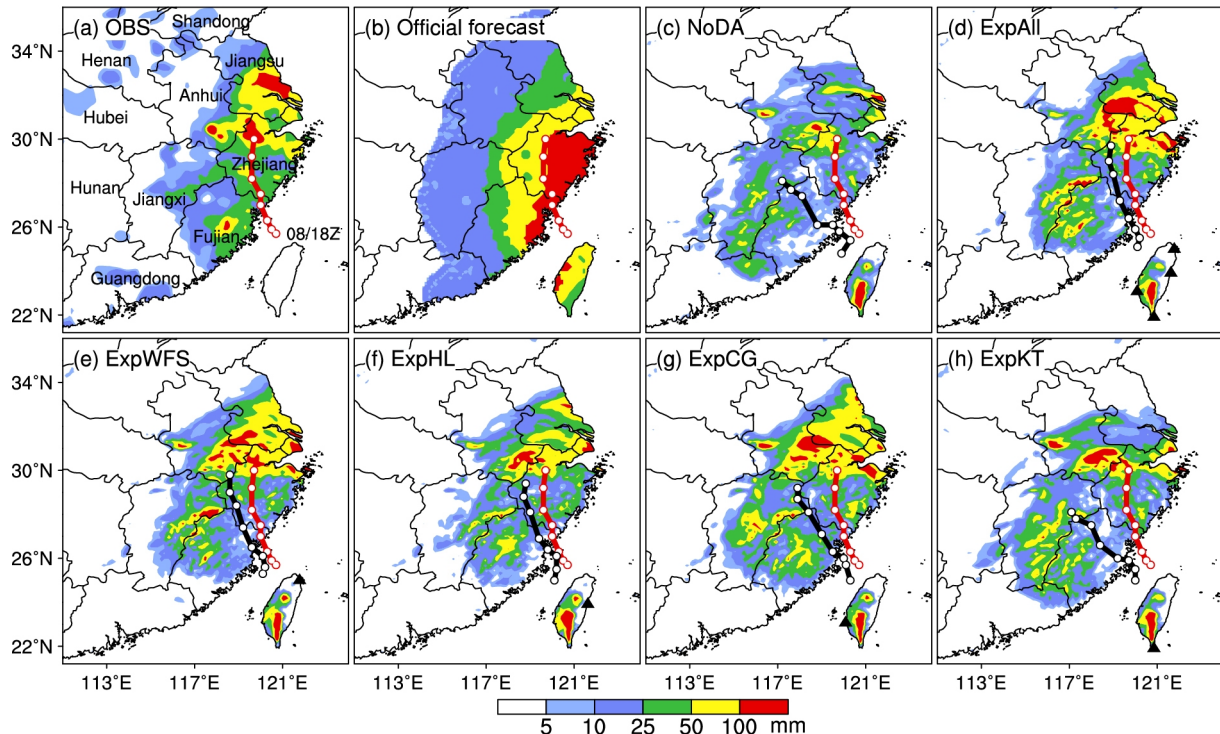


Figure 1 Observational analysis of the 24-h rainfall (mm) valid at 1200 UTC 10 August 2009 in the Chinese mainland (a), the official forecast issued by CNMC (b), the corresponding forecast of NoDA (c), and the deterministic forecast initiated from the EnKF analysis in ExpAll (d), ExpWFS (e), ExpHL (f), ExpCG (g), and ExpKT (h). The red and black lines with white dots represent the observed and simulated TC tracks, respectively, from 1800 UTC 8 August to 1200 UTC 10 August. The triangles denote the locations of the assimilated radars.

and Jiangsu Provinces (Figure 1a). In particular, the Yangtze River Delta region recorded large areas where 24-h (1200 UTC 09 August–1200 UTC 10 August) rainfall amounts exceeded 50 mm.

2.2 Doppler radar data in Taiwan

Due to its slow translation speed and large size, Morakot was observed clearly by Taiwan's coastal radars, even 12 h after it departed from Taiwan (Figure 2). The Vr data used in this study were collected by four S-band (10 cm) coastal Doppler radars, which are operated by the Taiwan's Central Weather Bureau (CWB) of China. These radars are located at Wu-Fen-Shan (WFS), Ken-Ting (KT), Hua-Lien (HL), and Chi-Gu (CG) sites (Figure 2) and have a 230 km maximum Vr measurement range and nine elevation angles between 0.5° and 19.5°. Due to the mountainous topography in Taiwan, part of the lower scans of the HL and KT radars and the eastern outer range of the CG radar are blocked. Because the

WFS radar is located at the top of a mountain, it has better data coverage than the other three radars. In addition, Morakot took a northwest track during and after its landfall in Taiwan; thus, the northernmost WFS radar had the best TC inner-core coverage.

3. Assimilation method and experimental design

3.1 WRF and EnKF

The Advanced Research WRF (ARW) model (Skamarock et al., 2008), version 3.6.1, was used in this study. Three domains with two-way nesting were used for the analyses and forecasts (Figure 3). The coarsest domain (D1) had 150 × 120 horizontal grid points and a grid spacing of 40.5 km, the second domain (D2) had 187 × 199 grid points and a grid spacing of 13.5 km, and the innermost domain (D3) had 226 × 391

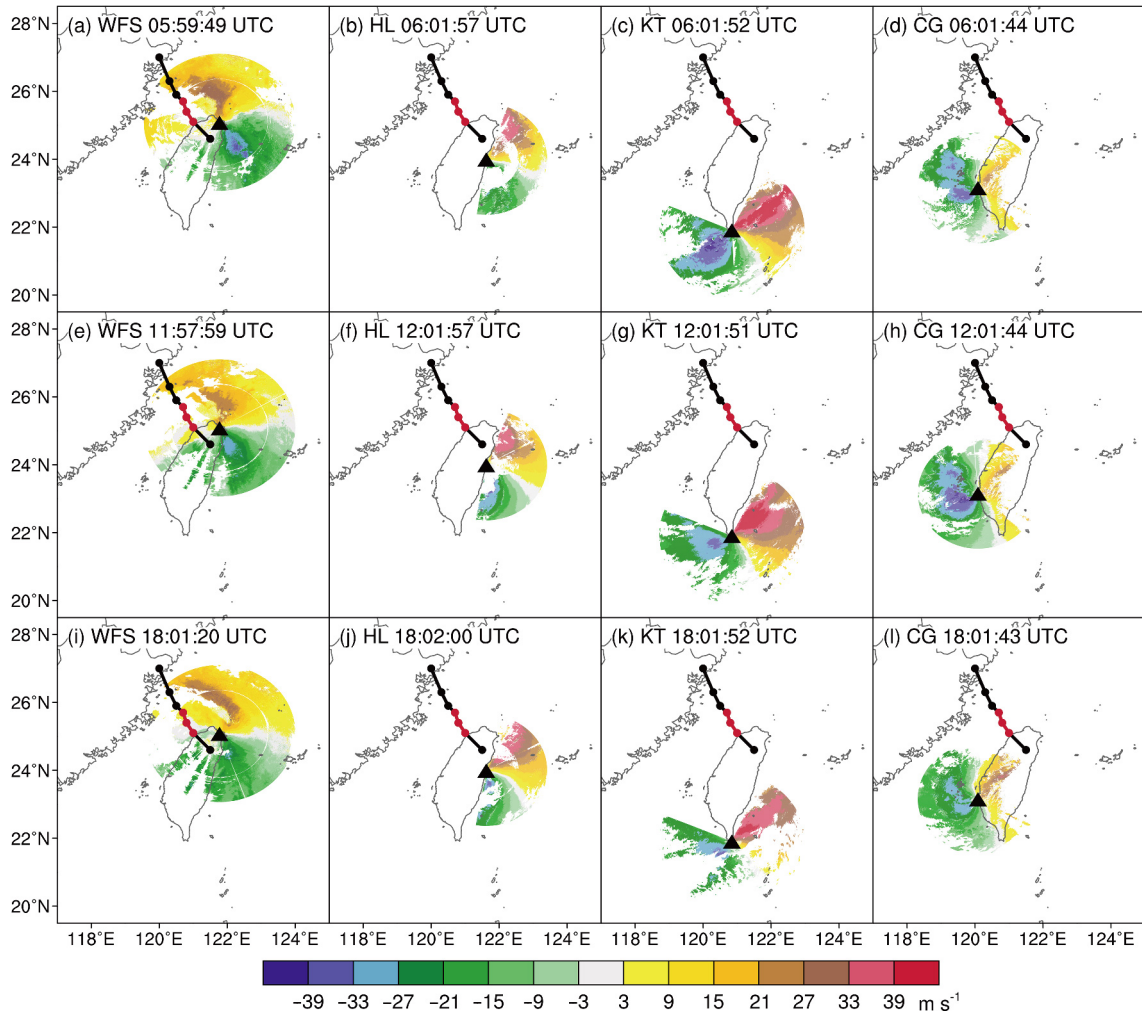


Figure 2 Distribution of Vr (m s^{-1}) at an elevation angle of 0.5° for ((a), (e), (i)) WFS, ((b), (f), (j)) HL, ((c), (g), (k)) KT, and ((d), (h), (l)) CG at around (from upper to lower) 0600, 1200, and 1800 UTC 8 August 2009. The location of each radar (black triangles) and the 6-hourly CWB best track from 0000 UTC 8 August to 1200 UTC 9 August (red segments denote the assimilation period) are also plotted.

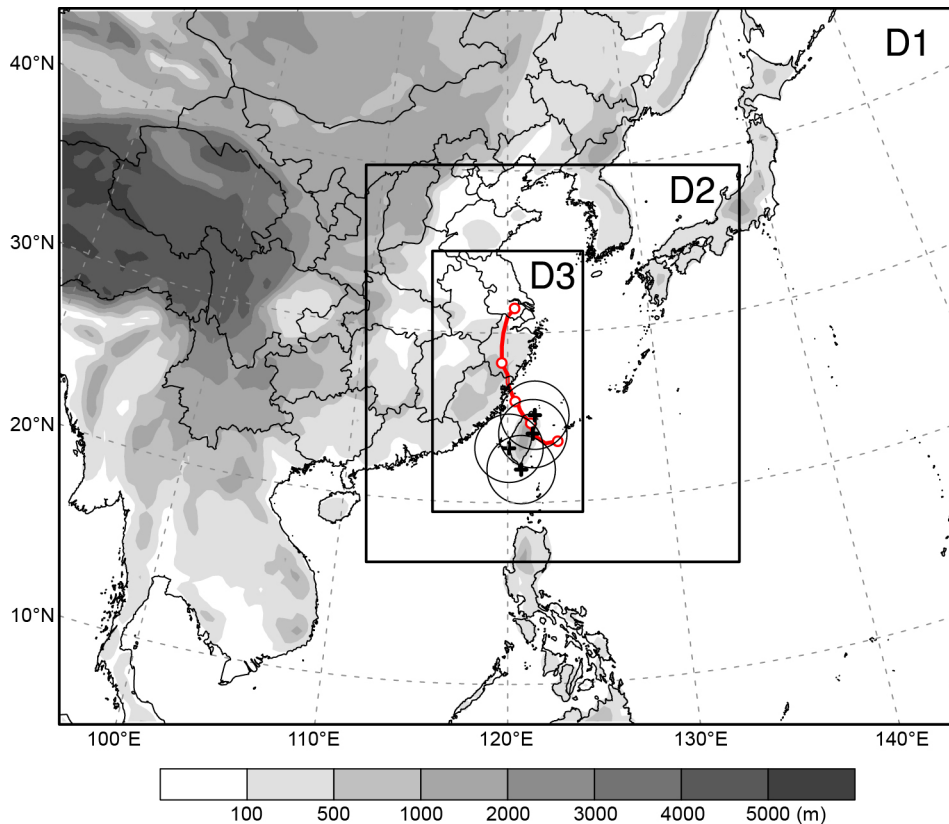


Figure 3 Model domain configuration. The red line denotes the CWB best track from 0000 UTC 7 August to 0000 UTC 11 August 2009. All the positions at 0000 UTC are marked by a white dot. Also shown are the location (black crosses) and maximum Doppler range (black circles) of the four operational radars in Taiwan. The gray shading shows the terrain height (m).

grid points and a grid spacing of 4.5 km. All domains had 35 vertical layers, and the model top was set at 10 hPa. The physical parameterization schemes included the Grell–Devenyi ensemble cumulus scheme (Grell and Devenyi, 2002) for the two coarse domains (D1 and D2), the WRF Single-Moment six-class microphysics with graupel (Hong et al., 2004), and the Yonsei State University scheme (Noh et al., 2003) for planetary boundary layer processes. The National Centers for Environmental Prediction (NCEP) Global Forecast System (GFS) operational analysis and forecast were used to generate the initial and lateral boundary conditions.

The WRF-based EnKF system used in this study is the same as that in Z09 except that 60 ensemble members were used. This version of the filter was originally developed for regional scale DA, which was documented by Meng and Zhang (2008a, 2008b). The covariance relaxation method (Zhang et al., 2004) was used to prevent filter divergence. This method inflates the covariance via a weighted average between the prior perturbation (denoted by superscript f) and the posterior perturbation (denoted by superscript a) as $(x_{new}^a)' = (1 - \alpha)(x^a)' + \alpha(x^f)',$ where α is the weighting coefficient. As in Z09, α is necessary to be 0.7 to 0.8 for real-data applications due to unavoidable imperfections in the forecast model, so α was set to 0.8 in this study, which was the same as in Z09. In real-data applications, the

posterior ensemble spread tends to be much smaller than the observational error. Thus, a larger weight is given to the prior perturbation, which has a larger ensemble spread than the posterior perturbation, to inflate the background error covariance more efficiently. The initial ensemble was generated with the WRF-3DVar system by using the NCEP cv3 background error covariance (Barker et al., 2004). The domain-averaged standard deviations of the perturbations were approximately 2 m s^{-1} for horizontal wind components (u, v), 1 K for potential temperature, 1 hPa for pressure perturbation, and 0.5 g kg^{-1} for water vapor mixing ratio.

Because the resolution of radar observations was much higher than the forecast model grid spacing, superobservations (SOs) were generated with a resolution of 5 km in the radial direction and 5° in the azimuthal direction for significant data thinning. As in Z09, the quality-controlled Vr SOs were assimilated by using the successive covariance localization (SCL) method with a horizontal localization radius of influence (ROI) of 1215, 405, and 135 km for D1, D2, and D3, respectively. The ROI in the vertical direction was set to the model depth.

3.2 Experimental design

The impact of assimilating Taiwan's radars that have various

TC coverage or data availability on the track and rainfall forecasts of Morakot after its landfall in southeastern China was examined. In the control experiment (Figure 4b), the NCEP GFS operational analysis at 0000 UTC 8 August 2009 was used to generate an initial ensemble, followed by a 6-h ensemble forecast to develop a flow-dependent background error covariance structure that was approximately realistic. SOs from all four radars were then assimilated hourly from 0600 to 1800 UTC 8 August, over the 12 h after Morakot left Taiwan. At the end of the assimilation window, a deterministic forecast was initiated from the ensemble mean of the EnKF analyses until 1200 UTC 10 August, including the 24 h after Morakot's landfall in southeastern China. The control experiment is referred to as ExpAll. Four other experiments, called ExpWFS, ExpHL, ExpCG, and ExpKT, were conducted in the same way as ExpAll except that Vr data from a single radar at WFS, HL, CG, or KT, respectively, were assimilated. As a benchmark, the experiment NoDA was initiated from the NCEP GFS analysis at 0000 UTC 8 August without assimilating any observations (Figure 4a).

4. Comparison of assimilating Vr data from four radars vs a single radar

4.1 Control experiment

Assimilating Vr data from all four Taiwan's coastal radars improved the TC center position and structure for the final EnKF analysis. In this study, the TC center was defined as the TC circulation center at the 850-hPa pressure level. In

ExpAll, the position error of the simulated TC center was reduced from 128.4 km in NoDA to 89.9 km (Figure 5b and 5c). The simulated radar reflectivity was also improved in ExpAll, with a more realistic pattern of both the strong convection to the east of Taiwan and the intense rainband, which extended from the Taiwan Strait to southwestern Taiwan (Figure 5a–c). Moreover, the EnKF analysis captured the TC mesoscale circulation much better than NoDA, as shown by comparing the 0.5° base scan of Vr at the WFS radar among the observation, NoDA, and ExpAll (Figure 6a–c).

ExpAll produced a better prediction of the TC track compared with NoDA (Figure 7a and 7b) owing to the improved environmental field, especially the steering flow at the end of the assimilation window. The steering flow was defined as the pressure-weighted average wind from 500 to 200 hPa within an annulus between 200 and 500 km from the TC center, similar to Chien and Kuo (2011). Both the western North Pacific

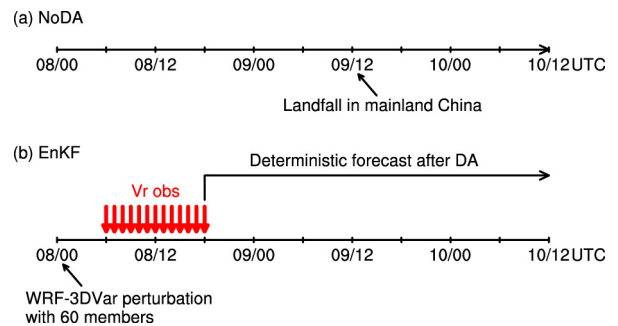


Figure 4 Schematic flow chart for NoDA (a) and EnKF (b) experiments.

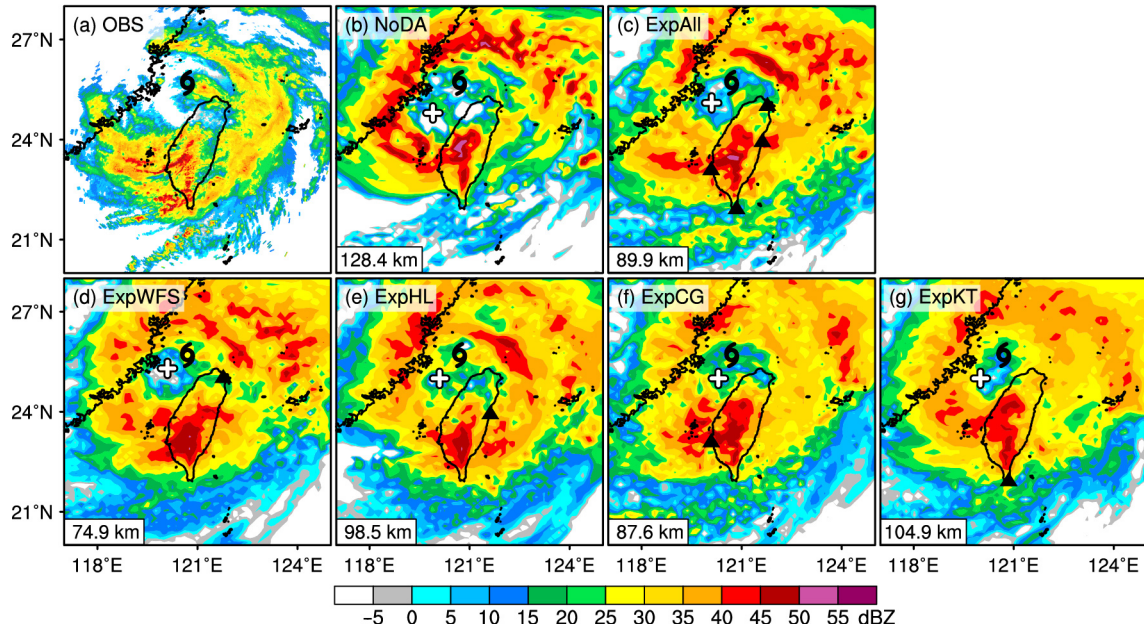


Figure 5 Distribution of maximum radar reflectivity (dBZ). (a) The observational composite mosaic at 1800 UTC 8 August 2009 and the distributions simulated by NoDA (b), ExpAll (c), ExpWFS (d), ExpHL (e), ExpCG (f), and ExpKT (g). The typhoon symbol and white cross in the panels denote the observed and simulated TC center, respectively. The TC center position error of each experiment is shown at the bottom left corner. The black triangles represent the locations of the assimilated radars.

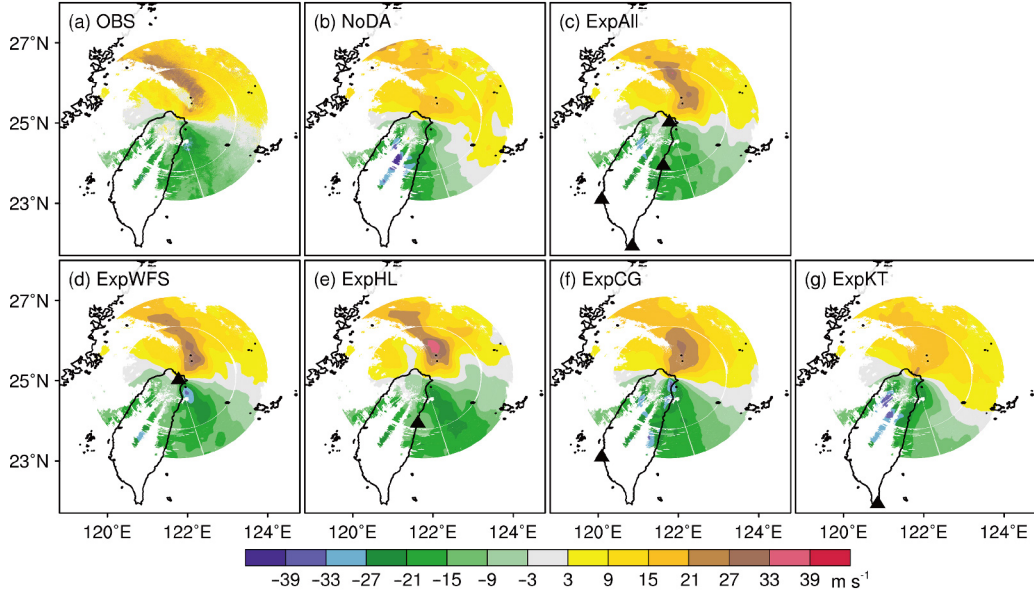


Figure 6 Distribution of V_r (m s^{-1}) at an elevation angle of 0.5° at the WFS radar. (a) The observation at 1800 UTC 8 August 2009 and the distributions simulated by NoDA (b), ExpAll (c), ExpWFS (d), ExpHL (e), ExpCG (f), and ExpKT (g). The black triangles in the panels denote the locations of the assimilated radars.

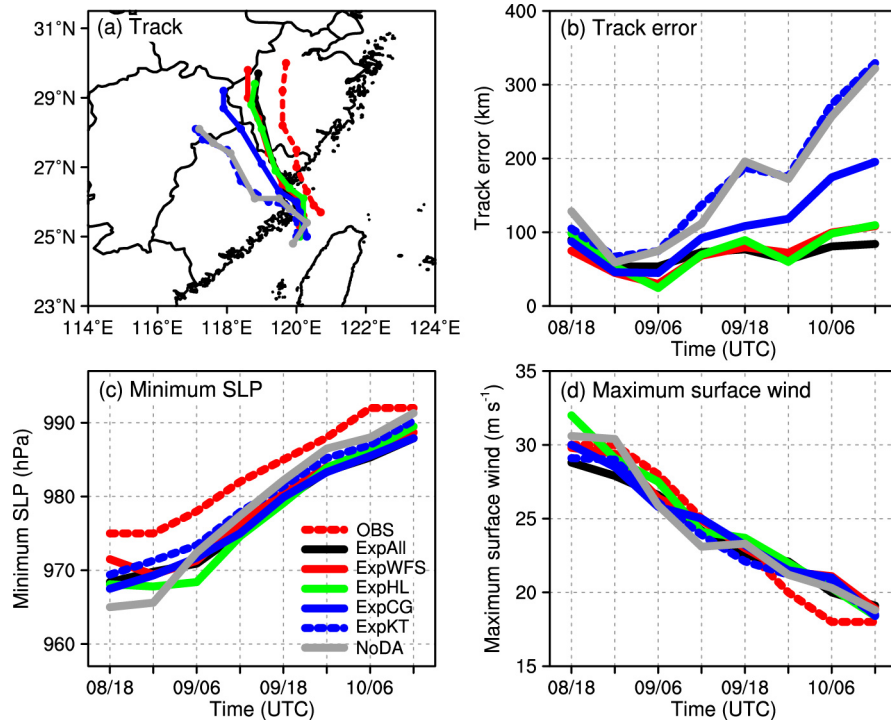


Figure 7 Predicted 6-hourly TC track (a), track error (b), minimum SLP (c), and maximum surface wind (d) from 1800 UTC 8 August to 1200 UTC 10 August 2009 in all experiments, along with the CWB best track estimate. The legend is shown in (c).

subtropical high and the high pressure system to the northwest of the TC in ExpAll were closer to the European Center for Medium-Range Weather Forecasts interim reanalysis (ERA-Interim; Dee et al., 2011), resulting in a better initial steering flow (Figure 8a). Assimilating V_r data also improved the TC intensity forecast during the first few hours of the integration (Figure 7c and 7d), although the improvements were

short-lived. There were no apparent differences among the experiments thereafter. This was likely due to the dominance of forecast error because of deficiencies in the forecast model (e.g., physics and resolution). The limited improvement in the single-radar DA experiments may also be caused by only assimilating V_r from a single radar.

In addition to the track forecast, assimilating V_r data also

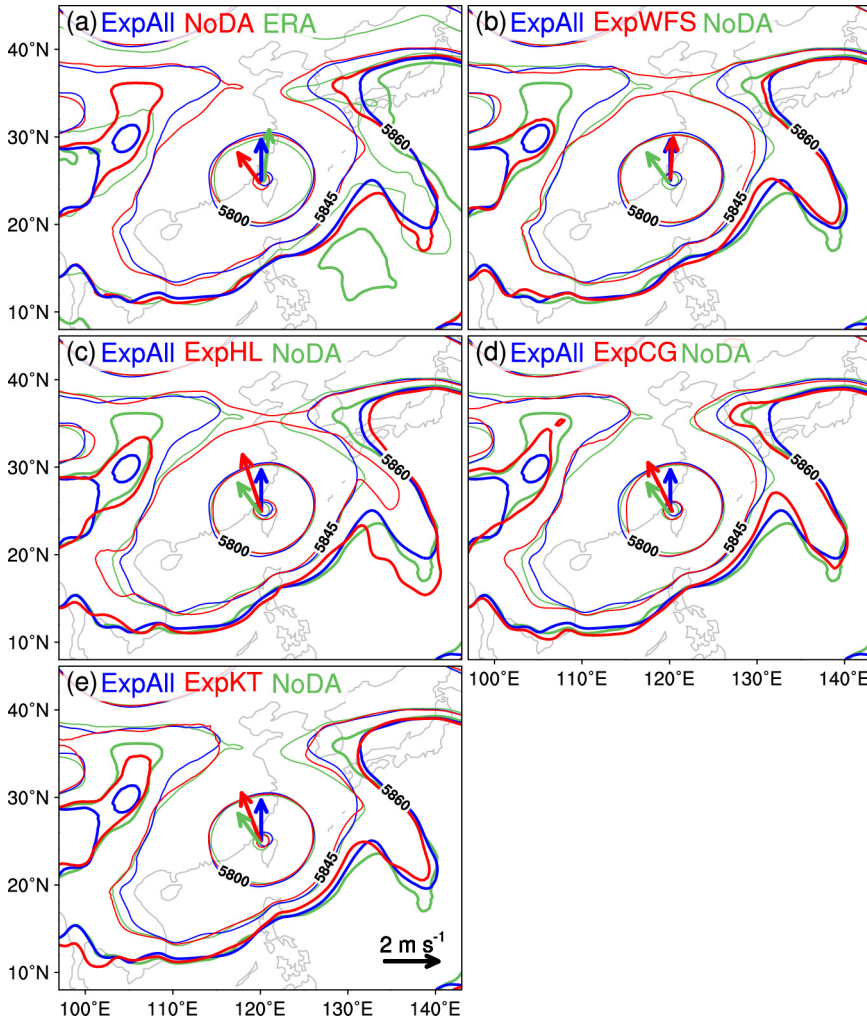


Figure 8 Comparison of geopotential height at 500 hPa (contour levels: 5660, 5800, 5845, and 5860 m; thick contour for 5860 m) and steering flow (vector) among ExpAll, NoDA, and ERA-Interim (a), ExpWFS (b), ExpHL (c), ExpCG (d), and ExpKT (e) at 1800 UTC 8 August 2009. The reference vector is shown at the bottom right corner of (e).

had a large impact on the TC rainfall forecast. Observations showed that large areas of coastal regions suffered heavy rainfall, especially in northern Zhejiang and southern Jiangsu (Figure 1a). NoDA provided a poor forecast of the rainfall pattern and amount, which may be due to its large track error (Figure 1c). In contrast, a significant improvement in the TC track and rainfall pattern was obtained in ExpAll (Figure 1d). In particular, the observed heavy rainfall exceeding 50 mm was captured, though with a slight southward bias. Consequently, ExpAll had a consistently higher threat score than NoDA for different thresholds (10, 25, 50, and 100 mm; Figure 9).

Although the Vr observations were only taken near the TC center before the TC made landfall in mainland China, the largest improvement in the 24-h rainfall was mainly seen far from where data were assimilated (Figure 1a, 1c, and 1d). This improvement in long-distance rainfall was obtained mainly through the improved TC position (Figure 7b) and structure (Figure 6a–c) as well as the improved environmen-

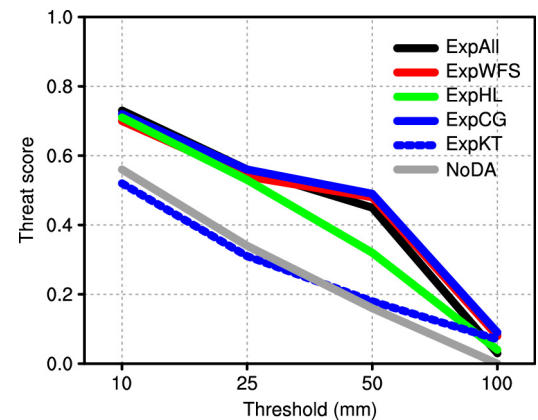


Figure 9 Threat score of 24-h rainfall for different thresholds valid at 1200 UTC 10 August 2009 in NoDA and deterministic forecasts initiated from the EnKF analyses.

tal field, especially the steering flow (Figure 8a) at the end of the assimilation window, which resulted in the subsequent improved TC track forecast (Figure 7a and 7b). After the first

DA, only the area around the assimilated data was affected (Figure 10a and 10b). However, as the number of cycles of forecast and assimilation increased, the affected area was much larger at the end of the assimilation window (Figure 10c). Because the earlier tracks were close to each other, the rainfall forecasts were similar for ExpAll and NoDA (Figure 11b and 11c). With the improved track forecast later on, an apparent improvement in rainfall forecast was observed in ExpAll compared with NoDA (Figure 11d–i), probably because of the more accurate moisture convergence near the observed rainfall area at later times (Figure 10d–f).

4.2 Impact of assimilating single-radar data at different locations

Compared with NoDA, assimilating single-radar data also

improved the position of the TC center to different degrees owing to their different coverage of the TC inner core. In the final EnKF cycle, the TC center position in all four single-radar DA experiments got closer to the observation than NoDA (Figure 5, the position errors are given at the bottom left corner of each panel). ExpWFS had the smallest initial TC center position error of about 75 km, followed by ExpCG, ExpHL, and ExpKT. Notably, the initial TC center position error in ExpWFS was even smaller than that in ExpAll. This result indicates that assimilating additional radar Vr data may provide limited improvement over what is obtained by assimilating the Vr data from a radar with good TC inner-core coverage (Figure 2).

Assimilating Vr data from a single radar at different locations relative to Morakot can improve the TC structure to different degrees at the end of the assimilation window. The ob-

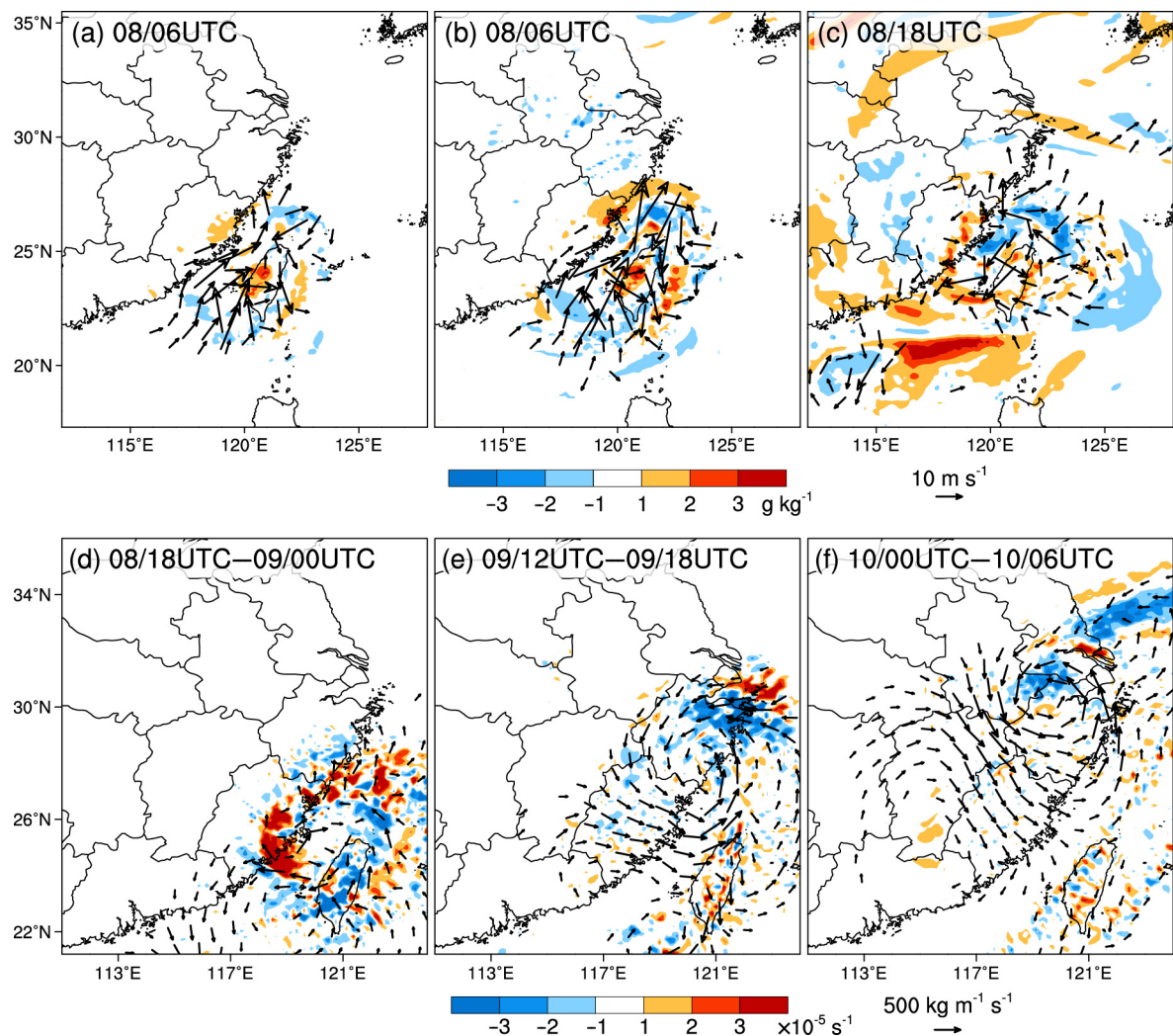


Figure 10 Difference in water vapor mixing ratio at 700 hPa (shaded, g kg^{-1}) and horizontal wind at 850 hPa (larger than 5 m s^{-1} , reference vector at lower right) between the posterior in ExpAll and (a) the prior, (b) NoDA at 0600 UTC 8 August 2009, and that between the posterior in ExpAll and (c) NoDA at 1800 UTC 8 August. Also shown are the evolution of the 6-h averaged vertically integrated (from surface to 500 hPa) moisture flux difference between ExpAll and NoDA (larger than $1.5 \times 10^2 \text{ kg m}^{-1} \text{s}^{-1}$, reference vector at lower right) and its divergence (shaded, s^{-1}) valid at (d) 0000 and (e) 1800 UTC 9 August, and (f) 0600 UTC 10 August.

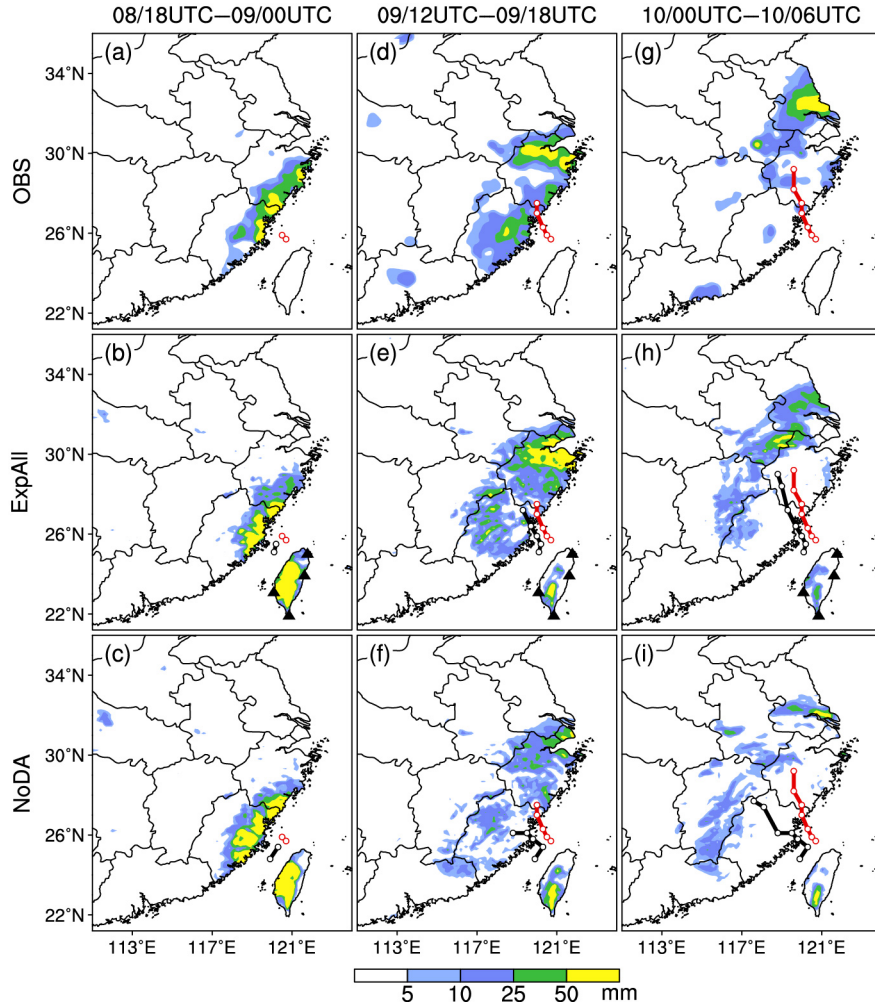


Figure 11 6-h rainfall (mm) predicted by ((b), (e), (h)) ExpAll and ((c), (f), (i)) NoDA, compared with ((a), (d), (g)) the observational analysis valid at (from left to right) 0000 and 1800 UTC 9 August and 0600 UTC 10 August 2009. The red and black lines with dots represent the best track estimate and the simulated TC track from 1800 UTC 8 August to the end of the corresponding rainfall period, respectively. The triangles in ((b), (e), (h)) denote the locations of the assimilated radars.

served intense reflectivity in the southern and eastern quadrants of the storm was better captured by all the single-radar DA experiments compared with NoDA (Figure 5). In particular, a more realistic intense rainband around southwestern Taiwan was observed in ExpWFS in terms of the location and morphology. The pattern of simulated Vr at an elevation angle of 0.5° at the WFS radar was also improved in all the single-radar DA experiments, except for ExpKT, with the best agreement with observation obtained in ExpWFS (Figure 6). Nevertheless, the morphology and intensity of Vr exceeding 21 m s^{-1} was poorly simulated in ExpCG and ExpHL, respectively.

Generally, a more accurate initial TC center position tended to produce a more accurate track forecast. The simulated tracks of ExpWFS and ExpHL were similar to that of ExpAll (Figure 7a), except that they both produced a smaller track error at an earlier stage and a larger track error after 0000 UTC 10 August compared with ExpAll (Figure 7b). ExpCG showed a larger track error growth, although its initial TC

center had a smaller position error than ExpHL and a similar position error to ExpAll. Similar to NoDA, the TC in ExpKT deviated west-northwestward after landfall with a track error exceeding 200 km for the last 6 h of the simulation. The experiments that predicted a better TC track than NoDA all produced a better 24-h rainfall forecast after TC landfall in southeastern China (Figures 7a, 7b, and 9). ExpKT showed the worst performance; thus, the performance of ExpAll would be slightly better if the KT radar data were not assimilated.

5. Why assimilating different radar data has different impacts on TC track and rainfall forecasts

The better predicted tracks in ExpAll, ExpWFS, and ExpHL (Figure 7a) were probably associated with better environmental field and steering flow, especially at the beginning of the deterministic forecast. As in Section 3.1, the geopotential

height at 500 hPa and the steering flow at 1800 UTC 8 August were also examined in all the single-radar DA experiments. The results showed that the key difference was in the ridge of the high pressure system to the northwest of the TC, which can be clearly seen in the 5860 m contour. ExpWFS was similar to ExpAll in terms of the initial 5860 m contour and steering flow (Figure 8b), contributing to their similar better predicted tracks. The initial steering flow in the other three single-radar DA experiments pointed less northward than that in ExpAll and more northward than that in NoDA (Figure 8c–e), probably because of the stronger high pressure system to the northwest of the TC in terms of the larger extent of the 5860 m contour. The accuracy of the 5860 m contour

at around 30°N, 100°E was in the order ExpHL > ExpCG > ExpKT, and was quite consistent with their track forecast errors. After landfall, the intensifying steering flow in ExpAll, ExpWFS, and ExpHL persistently pointed more northward than those in other experiments, and thus was more similar to that derived from ERA-Interim reanalysis data, resulting in the similar northward TC motion and smaller track error (Figures 12 and 13).

Assimilating Vr data that had different coverage of the TC inner core also caused different impacts on the TC track and rainfall forecasts. An important reason why ExpWFS had the best performance was probably that the WFS radar had the best TC inner-core coverage compared with the other three

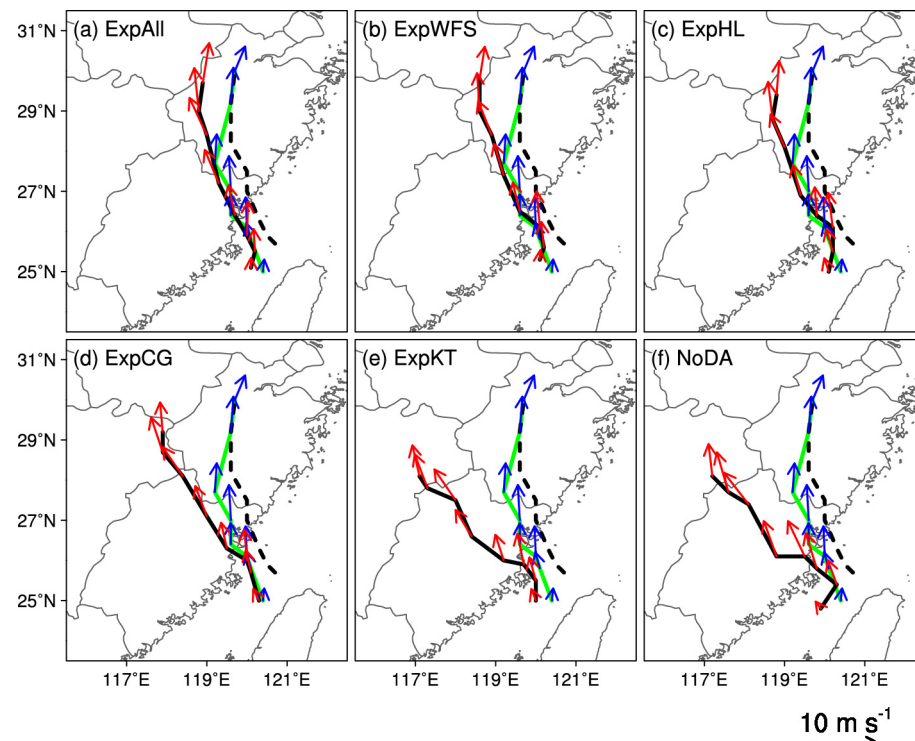


Figure 12 Steering flow (red arrows) in ExpAll (a), ExpWFS (b), ExpHL (c), ExpCG (d), ExpKT (e), and NoDA (f) during 1800 UTC 8 August–1200 UTC 10 August 2009. The black solid and dashed lines represent the simulated and observed TC tracks, respectively. The TC track (green solid line) and steering flow (blue arrows) derived from ERA-Interim reanalysis data are also plotted for verification.

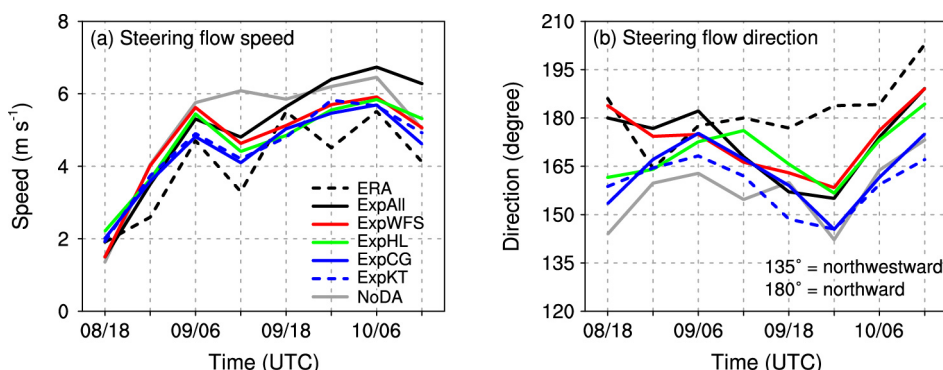


Figure 13 Evolution of steering flow (a) speed (m s^{-1}) and (b) direction (degree) during 1800 UTC 8 August–1200 UTC 10 August 2009 in all experiments and ERA-Interim reanalysis data. The legend and referential directions are shown in (a) and (b), respectively.

radars (Figure 2). Although ExpHL had a similar track to ExpWFS, it had a less accurate 24-h rainfall pattern and amount forecast after landfall (Figures 1a, 1e, 1f, and 9), probably because the HL radar could not observe the TC inner core properly, resulting in a less realistic initial TC structure (Figure 6a,

6d, and 6e). This may have led to the significant divergence of the low- and mid-level moisture flux difference between ExpHL and ExpWFS in Zhejiang and Jiangsu provinces, especially for the first 18 h after landfall (Figure 14), causing the underprediction of the rainfall amount in ExpHL. ExpCG

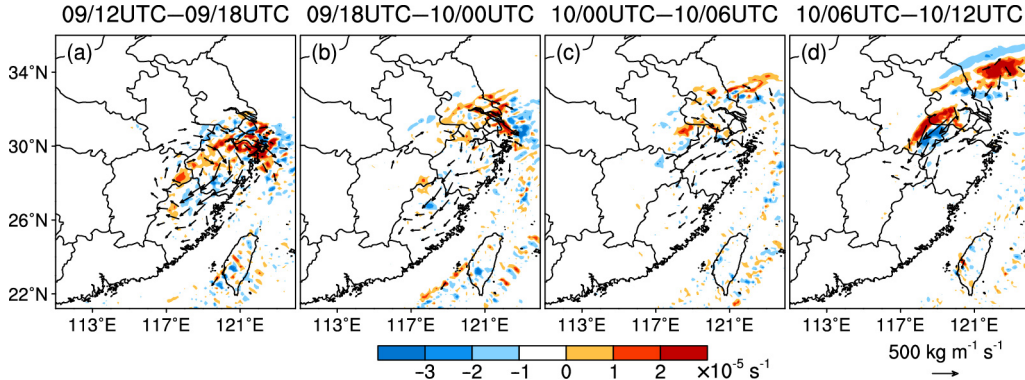


Figure 14 Evolution of the 6-h averaged vertically integrated (from surface to 500 hPa) moisture flux difference between ExpHL and ExpWFS (larger than $1.5 \times 10^2 \text{ kg m}^{-1} \text{ s}^{-1}$, reference vector at lower right) and its divergence (shaded, s^{-1}) valid at (a) 1800 UTC 9 August, and (b) 0000, (c) 0600, and (d) 1200 UTC 10 August 2009.

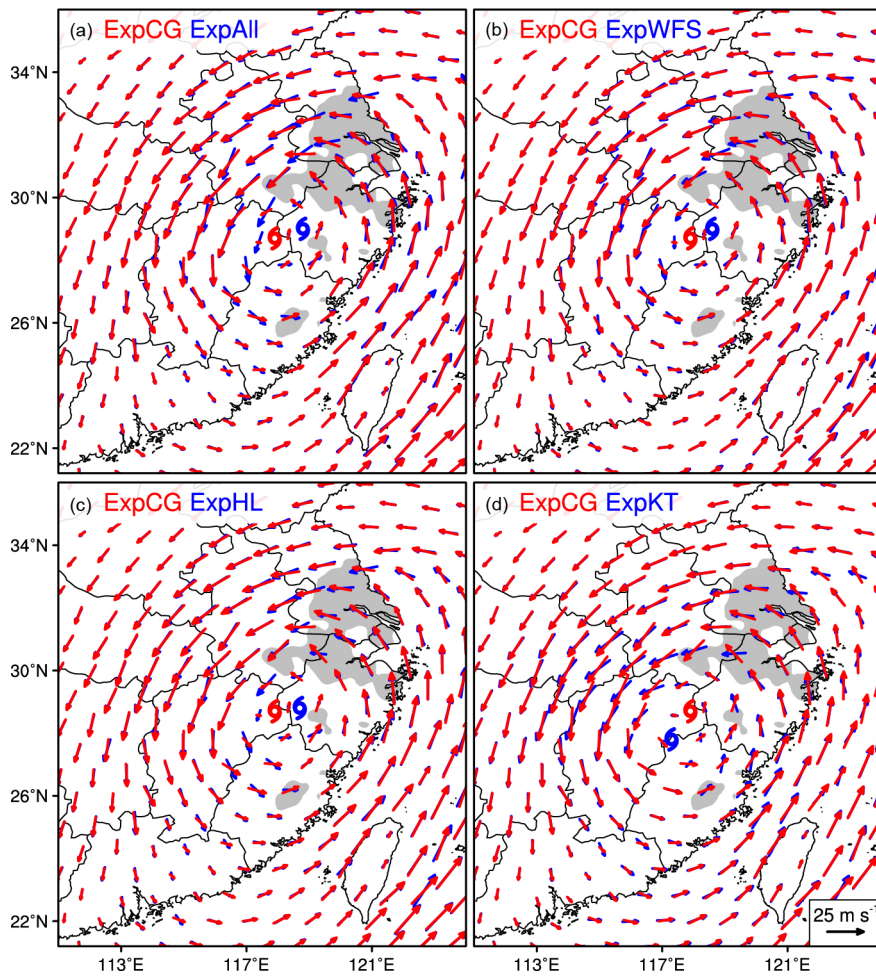


Figure 15 Comparison of horizontal wind at 850 hPa between ExpCG and ExpAll (a), ExpWFS (b), ExpHL (c), and ExpKT (d) at 0600 UTC 10 August 2009. The gray area denotes the region of the observed 24-h rainfall after Morakot's landfall exceeding 50 mm. The corresponding TC positions are labeled with typhoon symbols. The reference vector is shown at the bottom right corner of (d).

had a more skillful rainfall forecast, but a larger track forecast error than ExpAll, ExpWFS, and ExpHL, possibly because assimilating the CG radar data did not improve the steeringflow at the initial time, but increased the low-level convergence in the observed rainfall area during the forecast period (Figure 15a–c). ExpCG had a better rainfall forecast than ExpKT, although they both had a large westward bias in the track forecast for the same reason (Figure 15d). This result indicates that assimilating Vr data from a radar that has poor TC inner-core coverage may not guarantee a consistent improvement in TC track and rainfall forecasts.

6. Conclusions

This study explored for the first time the impact of assimilating Vr observations from a single or multiple Taiwan's coastal radars on the track and rainfall forecasts after a TC makes landfall in the Chinese mainland by using a WRF-based EnKF DA system. The case that was examined was Typhoon Morakot (2009), which made landfall in southeastern China after passing through northern Taiwan and caused widespread damage in coastal regions.

The final EnKF analysis with cycled assimilation of Vr data produced a vortex that had a more realistic TC position and structure. The largest error reduction of the initial TC center position was obtained by assimilating data from the radar that had the best TC inner-core coverage. Assimilating this single-radar data may produce a similar or even better performance than assimilating additional data from radars with poorer coverage of the TC inner core. Different radars might have played different roles depending on the TC's track, such as corrections for the TC inner-core structure, the environmental field, and moisture. Deterministic forecasts initiated from more realistic EnKF analyses improved the TC track and rainfall forecasts. In particular, Taiwan's radars that observed the TC inner core better tended to make a larger contribution to the rainfall forecast in the mainland of China. However, the impact of assimilating Vr data on the TC intensity forecast was not substantial after about 12 h into the integration, possibly because only the Vr instead of the full wind was assimilated.

Considering that this study was only based on Typhoon Morakot (2009), it is necessary to confirm the findings by examining more cases. Nevertheless, the promising results in the current study demonstrate the great potential of assimilating radar data from Taiwan in improving track and rainfall forecasts of the TCs that make landfall in the Chinese mainland after passing over or near Taiwan of China.

Acknowledgements The authors are very grateful to Yu ChengKu and Cheng LinWen for their technique support and helpful comments. This research was sponsored by the Special Fund for Meteorological Research in the Public Interest from the Ministry of Science and Technology of China

(Grant No. GYHY201306004), the National Key Basic Research Program of China (Grant No. 2013CB430104), and the National Natural Science Foundation of China (Grant Nos. 41461164006, 41425018 & 41375048).

References

- Barker D M, Huang W, Guo Y R, Bourgeois A J, Xiao Q N. 2004. A three-dimensional variational data assimilation system for MM5: Implementation and initial results. *Mon Weather Rev*, 132: 897–914
- Chien F C, Kuo H C. 2011. On the extreme rainfall of Typhoon Morakot (2009). *J Geophys Res*, 116: D05104
- Dee D P, Uppala S M, Simmons A J, Berrisford P, Poli P, Kobayashi S, Andrae U, Balmaseda M A, Balsamo G, Bauer P, Bechtold P, Beljaars A C M, van de Berg L, Bidlot J, Bormann N, Delsol C, Dragani R, Fuentes M, Geer A J, Haimberger L, Healy S B, Hersbach H, Hölm E V, Isaksen L, Källberg P, Köhler M, Matricardi M, McNally A P, Monge-Sanz B M, Morcrette J J, Park B K, Peubey C, de Rosnay P, Tavolato C, Thépaut J N, Vitart F. 2011. The ERA-Interim reanalysis: Configuration and performance of the data assimilation system. *Q J R Meteorol Soc*, 137: 553–597
- Dong J, Xue M. 2013. Assimilation of radial velocity and reflectivity data from coastal WSR-88D radars using an ensemble Kalman filter for the analysis and forecast of landfalling hurricane Ike (2008). *Q J R Meteorol Soc*, 139: 467–487
- Gao S, Meng Z, Zhang F, Bosart L F. 2009. Observational analysis of heavy rainfall mechanisms associated with severe tropical storm Bilis (2006) after its landfall. *Mon Weather Rev*, 137: 1881–1897
- Grell G A, Dévényi D. 2002. A generalized approach to parameterizing convection combining ensemble and data assimilation techniques. *Geophys Res Lett*, 29: 38-1–38-4
- Hamill T M, Whitaker J S. 2005. Accounting for the error due to unresolved scales in ensemble data assimilation: A comparison of different approaches. *Mon Weather Rev*, 133: 3132–3147
- Hamill T M, Whitaker J S, Kleist D T, Fiorino M, Benjamin S G. 2011. Predictions of 2010's tropical cyclones using the GFS and Ensemble-Based data assimilation methods. *Mon Weather Rev*, 139: 3243–3247
- Hong S Y, Dudhia J, Chen S H. 2004. A revised approach to ice microphysical processes for the bulk parameterization of clouds and precipitation. *Mon Weather Rev*, 132: 103–120
- Houze R A, Chen S S, Smull B F, Lee W C, Bell M M. 2007. Hurricane intensity and eyewall replacement. *Science*, 315: 1235–1239
- Li Y, Wang X, Xue M. 2012. Assimilation of radar radial velocity data with the WRF hybrid ensemble-3DVAR system for the prediction of hurricane Ike (2008). *Mon Weather Rev*, 140: 3507–3524
- Meng Z Y, Zhang F Q. 2008a. Tests of an ensemble Kalman filter for mesoscale and regional-scale data assimilation. Part III: Comparison with 3DVar in a real-data case study. *Mon Weather Rev*, 136: 522–540
- Meng Z Y, Zhang F Q. 2008b. Tests of an ensemble Kalman filter for mesoscale and regional-scale data assimilation. Part IV: Comparison with 3DVar in a month-long experiment. *Mon Weather Rev*, 136: 3671–3682
- Noh Y, Cheon W G, Hong S Y, Raasch S. 2003. Improvement of the K-profile model for the planetary boundary layer based on large eddy simulation data. *Bound-Layer Meteorol*, 107: 401–427
- Skamarock W C, Klemp J B, Dudhia J, Gill D O, Barker D M, Duda M G, Huang X-Y, Wang W, Powers J G. 2008. A description of the Advanced Research WRF version 3. NCAR Tech Note TN-475+STR. 113
- Whitaker J S, Hamill T M, Wei X, Song Y, Toth Z. 2008. Ensemble data assimilation with the NCEP global forecast system. *Mon Weather Rev*, 136: 463–482
- Wu C C. 2013. Typhoon Morakot: Key findings from the journal TAO for improving prediction of extreme rains at landfall. *Bull Amer Meteorol Soc*, 94: 155–160
- Wu C C, Yang M J. 2011. Preface to the special issue on “Typhoon Morakot

- (2009): Observation, modeling, and forecasting". *Terr Atmos Ocean Sci*, 22: I
- Yu C K, Cheng L W. 2013. Distribution and mechanisms of orographic precipitation associated with Typhoon Morakot (2009). *J Atmos Sci*, 70: 2894–2915
- Zhang F, Snyder C, Sun J. 2004. Impacts of initial estimate and observation availability on Convective-Scale data assimilation with an ensemble Kalman Filter. *Mon Weather Rev*, 132: 1238–1253
- Zhang F, Weng Y, Sippel J A, Meng Z, Bishop C H. 2009. Cloud-resolving hurricane initialization and prediction through assimilation of Doppler Radar observations with an ensemble Kalman Filter. *Mon Weather Rev*, 137: 2105–2125
- Zhang M, Zhang F, Huang X Y, Zhang X. 2011. Intercomparison of an Ensemble Kalman Filter with Three- and Four-dimensional variational data assimilation methods in a limited-area model over the Month of June 2003. *Mon Weather Rev*, 139: 566–572
- Zhang Q, Liu Q, Wu L. 2009. Tropical cyclone damages in China 1983–2006. *Bull Amer Meteorol Soc*, 90: 489–495
- Zhao K, Xue M. 2009. Assimilation of coastal Doppler radar data with the ARPS 3DVAR and cloud analysis for the prediction of Hurricane Ike (2008). *Geophys Res Lett*, 36: L12803
- Zhao K, Li X, Xue M, Jou B J D, Lee W C. 2012. Short-term forecasting through intermittent assimilation of data from Taiwan and mainland China coastal radars for Typhoon Meranti (2010) at landfall. *J Geophys Res*, 117: D06108
- Zhao Q, Jin Y. 2008. High-resolution radar data assimilation for Hurricane Isabel (2003) at landfall. *Bull Amer Meteorol Soc*, 89: 1355–1372